PCCP
Physical Chemistry Chemical Physics

Accepted Manuscript

This article can be cited before page numbers have been issued, to do this please use: M. L. Grasso, J. Puszkiel, F. C. Gennari, A. Santoru, M. Dornheim and C. Pistidda, *Phys. Chem. Chem. Phys.*, 2020, DOI: 10.1039/C9CP05697A.

View Article Online
DOI: 10.1039/C9CP05697A

ARTICLE

CO_2 reactivity with Mg_2NiH_4 synthesized by *in situ* monitoring mechanical milling

Received 00th January 20xx,
Accepted 00th January 20xx

DOI: 10.1039/x0xx00000x

M.L. Grasso[a], J. Puszkiel[a,b,*], F.C. Gennari[a], A. Santoru[b], M. Dornheim[b], C. Pistidda[b]

CO_2 capture and conversion is a key research field for the transition towards an economy only based on renewable energy sources. In this regard, hydride materials are a potential option for CO_2 methanation since they can provide hydrogen and act as a catalytic species. In this work, Mg_2NiH_4 complex hydride is synthesized by *in situ* monitoring mechanical milling under hydrogen atmosphere from a $2MgH_2$:Ni stoichiometric mixture. Temperature and pressure evolution, as well as the characterization of the material during milling are monitored *in situ*, thus providing a good insight into the synthesis process. The cubic polymorph of Mg_2NiH_4 (S.G. *Fm*-3*m*) starts to be formed in the early beginning of the mechanical treatment due to the mechanical stress induced by the milling process. Then, after 25 hours of milling, Mg_2NiH_4 with monoclinic (S.G. *C*12/*c*1) structure appears. The formation of the monoclinic polymorph is most likely related to the stress release that follows the continuous refinement of the material's microstructure. At the end of the milling process, after 60 hours, the as-milled material is composed of 90.8 wt.% of cubic Mg_2NiH_4, 5.7 wt.% of monoclinic Mg_2NiH_4, and 3.5 wt.% of remnant Ni. The as-milled Mg_2NiH_4 shows high reactivity for the CO_2 conversion into CH_4. Under static conditions at 400 °C for 5 hours, the interactions between as-milled Mg_2NiH_4 and CO_2 result in the total CO_2 consumption and in the formation of the catalytic system Ni-$MgNi_2$-Mg_2Ni/MgO. Experimental evidence and thermodynamic equilibrium calculations suggest that the global methanation mechanism takes place through the adsorption of C and the direct solid gasification towards CH_4 formation.

1. Introduction

Methanation is a potential process to recycle waste CO_2 and hence to diminish the emissions of this greenhouse gas. The production of a chemical fuel such as methane offers two main benefits. Firstly, it allows using the energy from renewable sources during the off-peak periods to produce methane from CO_2 (Power-to-gas concept). Secondly, the energy can be chemically stored in an energy vector, which can then be distributed for heating, mobility, and other applications, using the already existing infrastructure[1,2]. The methanation reaction, commonly known as Sabatier reaction, is an exothermic (ΔH_{298K}= – 165 kJ mol^{-1}) and thermodynamically spontaneous (ΔG_{298K}= – 113.2 kJ mol^{-1}) reaction, described as follows[3]:

$$CO_{2(g)} + 4H_{2\,(g)} \longrightarrow CH_{4\,(g)} + 2H_2O_{(g)} \quad (1)$$

In order to achieve high reaction yields, high selectivity of conversion (i.e. CH_4), and appealing kinetic behavior of reaction (1), the presence of catalytic species such as transition metals (TM) is required[4-6]. One of the broadly used TM for methanation is Ni owing to its high activity, enhanced CH_4 selectivity and low cost. However, Ni-based catalysts have some constraints like deactivation caused by sintering and coke deposition as well as toxicological risks[7-11]. Selvam *et al.*[12,13] was the first to report on the possibility to use alloys and selected compounds (FeTi, $LaNi_5$, $CaNi_5$, Mg_2Cu, Mg_2Ni, and Mg_2NiH_4), commonly used for hydrogen storage, in CO_2 capture and conversion processes. For these materials, it was demonstrated that the possibility to form carbonates, hydroxides, and oxides on their surface improves the effectiveness of these material in the CO_2 conversion process. Among several alloys and compounds, Mg_2Ni and Mg_2NiH_4 have attracted attention for further investigations as potential heterogeneous catalysts for CO and CO_2 capture and conversion owing to the presence of Ni[14-16]. Mulas *et al.*[14] investigated as-milled Mg_2Ni-based catalysts for the conversion of CO under different mechanochemical conditions. A single mechanochemical step was first carried out, in which Mg_2Ni was exposed to $1CO:3H_2$ stoichiometric mixture. Then, a two-step mechanochemical process was carried out: a pre-hydrogenation process followed by treatment under CO atmosphere. The presence of metallic Ni, hydride species ($Mg_2NiH_{0.3}$ and Mg_2NiH_4), oxides (MgO and NiO) and carbides (Ni_3C and $MgNi_3C_x$) were detected in the solid product. In the gas phase, methane and ethane were obtained from the conversion of CO *via* the mechanochemical process catalyzed by Mg_2Ni. During milling, for this process, an induction period longer than 10 hours was observed. Kato *et al.*[15] investigated the catalytic properties of the surface of Mg_2NiH_4 for CO_2 methanation. Mg_2NiH_4 was synthesized from an elemental 2Mg:1Ni stoichiometric powder mixture by annealing at 500 °C for 24 hours under argon atmosphere followed by hydrogen cycling at 350 °C and 25 bar H_2. Thereafter, the Mg_2NiH_4–CO_2 interaction was studied upon hydrogen release from the complex hydride under CO_2 flow. The formation of oxides on the hydride surface precluded its full dehydrogenation, leading to a Mg_2NiH_{4-x} disproportionated surface, on which segregated MgO and Ni-clusters were formed. These Ni-clusters account for the catalytic activity of the hydride surface, leading to the dissociative adsorption of CO_2 and its subsequent methanation. In our recent work[16], Mg_2NiH_4 and Mg_2FeH_6

[a] Department of Physical Chemistry of Materials, Consejo Nacional de Investigaciones Científicas yTécnicas (CONICET) and Centro Atómico Bariloche, Av. Bustillo km 9500 S.C. de Bariloche, Argentina.
[b] Institute of Materials Research, Materials Technology, Helmholtz-Zentrum Geesthacht GmbH, Max-Planck Strasse 1, D-21502 Geesthacht, Schleswig-Holstein, Germany.

Electronic Supplementary Information (ESI) available: [details of any supplementary information available should be included here]. See DOI: 10.1039/x0xx00000x

synthesized by short milling and subsequent sintering were investigated as CO_2 capture and conversion media. These magnesium based-metal hydrides promoted the methanation of CO_2 at 400 °C and after 5 hours (Mg_2FeH_6) and 10 hours (Mg_2NiH_4). Based on the experiments performed under different conditions, it was possible to conclude that the methanation of CO_2 depends on the type of complex hydride, H_2:CO_2 mol ratio, temperature, and time. It was proposed that the global mechanism occurs through the reversed water-gas shift reaction followed by the methanation of CO in a steam atmosphere. Fe, Ni and Mg-Ni particles coming from the Mg_2FeH_6 and Mg_2NiH_4 decomposition, respectively, played a catalytic role on the global mechanism. Mg_2FeH_6 exhibits just a cubic structure (space group (S.G.): *Fm*-3*m*) in which the octahedral anion complexes $[FeH_6]^{4-}$ are surrounded by an eight-fold cubic configuration of Mg atoms[17]. Moreover, the decomposition of Mg_2FeH_6 in the inert atmosphere leads to the formation of free Mg , free Fe, and to the release of H_2. This decomposition behavior accounts for the lack of solubility of Fe and Mg[18]. Mg_2NiH_4 has two polymorphs. At low temperatures, this metal complex hydride exhibits a monoclinic structure (S.G.: *C*12/*c*1; LT: low temperature structure)[19]. However, above ~ 230 °C, the structure changes into an antifluorite cubic structure (S.G.: *Fm*-3*m*, HT: high temperature)[20-23]. This structural transformation is indeed strongly affected by internal stress induced by, for example, mechanical milling process or static compression upon heating process[24,25]. Moreover, the LT phase exists in two modifications: untwinned (LT1) and twinned (LT2). These modifications are present on the basic cell level, and the LT1/LT2 ratio depends on the thermal and mechanical history of the sample[19,26-28].

As recently reported[16], the as-synthesized Mg_2NiH_4 (short milling + sintering) with monoclinic structure made possible the full CO_2 capture and conversion after 10 hours. This process underwent *via* CO reduction with an active contribution of the direct reduction of CO_2 promoted by the formation of the MgH_2/Mg_2NiH_4 hydride system.

In this work, Mg_2NiH_4 is synthesized *via* ball milling. The main Mg_2NiH_4 polymorph in the as-milled material is the cubic one (S.G.: *Fm*-3*m*). Investigations on the Mg_2NiH_4-CO_2 system shows that upon dehydrogenation the full conversion of CO_2 occurs just in 5 hours and without the presence of CO. The global mechanism for the CO_2 capture and conversion are here investigated and compared at the light of the experimental evidences and supporting equilibrium thermodynamic calculations. Phase evolution, microstructural as well as morphological changes upon the milling process are also studied.

2. Experimental

2.1 Mechanical milling

5 g of 2MgH_2-Ni stoichiometric powder mixture (MgH_2: Rockwood Lithium, purity: 99.8% and Ni: Alfa Aesar, purity: 99%) was milled for 60 hours under about 20 bar of H_2 and at 500 rpm in a P6-Fritsch mill device. A stainless steel (S.S.) milling chamber of 200 cm^3 with internal pressure and temperature recorders located on the internal part of the chamber's lid and S.S. balls as grinding medium, with a ball to powder ratio of 10:1 were utilized. To assure reproducibility of the recorded pressure and temperature behavior, the milling process with the same amount of 2MgH_2:Ni powder mixture was done two times for 60 h without opening the milling chamber and three times stopping the process every 5 hours to take samples for characterization. The milling process was also performed with the empty chamber and in the same above described conditions in order to characterize the temperature and pressure variations in the absence of powder material.

2.2 Characterization

Powder X-ray diffraction method (PXD) was carried out in a Bruker D8 Discover diffractometer equipped with Cu X-ray source (λ = 1.54184 Å), operating at 50 kV and 1000 mA and a 2D VANTEC detector. A sample holder sealed with a poly(methyl methacrylate) (PMMA) dome was utilized to prevent the sample oxidation during PXD measurements, and diffraction patterns were collected from 10° to 95° and from 15° to 40° of 2θ. Information on the structural properties was taken from ICSD database[29] and the following Crystallographic Information Files CIFs files were used: # 0502260 (Mg, $P6_3/mmc$), # 161962 (MgH_2, $P4_2/mnm$), # 162411 (Mg_2Ni, P_6222), # 162412 (HT Mg_2NiH_4, *Fm*-3*m*), # 201606 (LT1 Mg_2NiH_4, *C*12/c1). Rietveld refinement was performed with the MAUD program in order to quantify the amounts of phases at different milling times[30,31]. The crystallite size of the phases present in the specimens was calculated with the Scherrer equation[32] using the following peaks: MgH_2 (2θ: 27.9°, (110)), Ni (2θ: 44.5°, (111)) and Mg_2NiH_4 (2θ: 39.3°). Scanning Electron Microscopy (SEM) observations and mapping analyses were performed in a ZEISS Crossbeam 340 microscope. Morphological analyses of powder samples dispersed on a carbon-based tape were performed with secondary electrons. Particle size distributions (PSDs) from the SEM observations of each material were calculated based on size measurements on every particle utilizing an interpolated polygon tool from iTEM software (License N° A2382500). The PSDs were calculated using 15 SEM photos. The values taken into account were those from mean diameter measurements.

Non-isothermal dehydrogenation measurements of the 2MgH_2-Ni stoichiometric powder mixture at different milling times were performed in a Sieverts device (HERA Hydrogen System) to characterize the hydrogen uptake of the material at different milling stages[33]. Each volumetric dehydrogenation measurement was done using about 150 mg of sample, heating up at about 3 °C/min from 25 °C to 400 °C under 1 bar of H_2. Thermal analyses of samples during milling were performed in an HP-DSC Netzsch DSC 204 HP calorimeter located inside an argon-filled glove box (H_2O and O_2 levels below 1 ppm). About 10 mg of samples were put in Al_2O_3 crucible and then heated up from room temperature to 400 °C with a heating ramp of 5 °C/min and at 1 bar of H_2 overpressure. The pressure was maintained constant through the overall measurement by the use of a mass flow meter. For each measurement, the chamber of the HP-DSC was flushed and evacuated three times with H_2 at room temperature.

CO_2 reactivity and conversion at the set temperature and pressure were assessed in a stainless steel reactor coupled to a Sieverts volumetric apparatus. A certain amount of as-milled Mg_2NiH_4 was introduced in the reactor and heated up to 400 °C at a heating ramp of 10 °C/min under CO_2 atmosphere and then kept isothermal for five hours. The amount of used as-milled

View Article Online
DOI: 10.1039/C9CP06544J

Mg_2NiH_4 was calculated to provide 4 mol of H_2, and to reach $4H_2$:$1CO_2$ at 1.2 bar in a volume of about 10 cm^3. After CO_2 interaction, the gaseous products were collected in a degassed quartz optical cell with KBr windows and then analyzed *via* Fourier-transform infrared spectroscopy in an FT-IR Perkin Elmer Spectrum series 400 spectrometer. Solid-phase products after CO_2 interaction were analyzed by Raman spectroscopy in order to identify carbon and carbon compounds in confocal microscope LabRAM HR Evolution Raman microscope at room temperature and using a laser wavelength of 514 nm.

2.3 Thermodynamic calculations

Thermodynamic equilibrium composition in an atmosphere of $4H_2$:$1CO_2$ ratio were calculated with the software HSC Chemistry 9.7[34]. The four moles of hydrogen were considered to be supplied by Mg_2NiH_4. The calculations were carried out at 400 °C, under a constant total pressure of 1.2 bar and variable pressure up to 1.2 bar, using a reaction volume of about 10 cm^3. These conditions are similar to the experimental ones. For these calculations under conditions similar to the experimental ones, the following phases were taken into account: $O_{2(g)}$, $CO_{(g)}$, $CO_{2(g)}$, $CH_{4(g)}$, $H_2O_{(g)}$, $C_2H_{4(g)}$, $C_2H_{6(g)}$, $CH_3OH_{(g)}$, and solid phases such as $Mg_2Ni_{(s)}$, $MgNi_{2(s)}$, $Ni_{(s)}$, $C_{(s)}$, $CO_3^{2-}{}_{(s)}$, $Mg_{(s)}$ and $MgO_{(s)}$.

3. Results

3.1 *In situ* monitoring mechanical milling process: Synthesis and characterization of Mg_2NiH_4

Fig. 1 shows the temperature and pressure evolution (Fig. 1A), as well as the phase evolution over the *in situ* monitoring mechanical milling process. As seen (Fig. 1A), the temperature rises about 18 °C during the first 15 hours and then remains constant till the end of the process. The pressure sharply increases about 1 bar within the first 2-3 hours, then notably decreases of about 0.5 bar in the following 15 hours, before rising to a final pressure of 0.6 bar. Rietveld analyses of samples taken at different stages of the milling process were performed (ESI:Fig. S1). Fig. 1A and Fig. 1B show the phase weight percentages (ESI: Table S1) and a graph with the total amounts of phases as well, respectively. At the beginning of the process (5 hours of milling), Ni, MgH_2, and free Mg are present in the material (Fig. 1B). The free Mg comes from the starting material (ESI: Fig. 2). In the specimens collected after the drop of pressure, cubic Mg_2NiH_4 (S.G. *Fm*-3*m*) is detected along with Ni and MgH_2. Further milling time (25 hours) results in the formation of untwinned monoclinic Mg_2NiH_4 (LT1, S.G. *C*12/*c*1, wt.%: 7.5±0.2). During this milling period, a notable increase of the amount of cubic Mg_2NiH_4 is also observed (S.G. *Fm*-3*m*, wt.%: 83.9±0.9). Between 25 hours and 45 hours, the amount of monoclinic Mg_2NiH_4 increases up to 29.1±1.0 wt.%. Finally, the monoclinic Mg_2NiH_4 (S.G. *C*12/*c*1) diminishes to 5.7±0.2 wt.% and the cubic Mg_2NiH_4 (S.G. *Fm*-3*m*) reaches 90.8±2.0. The final product of this synthesis, after 60 hours of milling, is composed of 3.5 wt.% of Ni and the total amount of Mg_2NiH_4 of 96.5±2.0 wt.%. These results obtained from the Rietveld analyses are in good agreement with the amount of Mg_2NiH_4 calculated from non-isothermal dehydrogenation volumetric measurements, taking into account a theoretical hydrogen capacity of 3.6 wt.% for Mg_2NiH_4 (ESI: Fig. S3): 89 wt.% of Mg_2NiH_4 after 25 hours and 92 wt.% of Mg_2NiH_4 after 60 hours.

PXD analyses in a short 2θ range (ESI: Fig. S2) and HP-DSC dehydrogenation experiments under 1 bar of H_2 (ESI: Fig. S4) support the evolution of the Mg_2NiH_4 polymorphs. In the HP-DSC analysis of the material milled five hours, the endothermic event with a peak maximum at about 275 °C accounts for MgH_2 decomposition catalyze by Ni (Fig. 1, ESI: Fig. S2, S4) in accordance with previous works[35,36].

The phase weight fractions reported in Fig. 1 and ESI: Fig. S2 do not show the presence of Mg_2NiH_4 after 15 hours of milling. The HP-DSC curve obtained for the material milled 15 hours, exhibits the endothermic peak ascribed to the decomposition of MgH_2 catalyzed by the presence of Ni (peak maximum ~275 °C) plus an endothermic shoulder at a lower temperature (~267 °C). As expected, the decomposition temperature (T_d) of Mg_2NiH_4 is lower than the T_d of MgH_2 (T_d for Mg_2NiH_4~250 °C and T_d for MgH_2~300 °C)[36,37]. Additionally, neither the early decomposition event of the LT1 phase below the phase transition temperature nor the LT to HT phase transition appears in the DSC curve[21,22,38], suggesting that the LT-Mg_2NiH_4 phase is not present. Thus, based on the Rietveld analyses, the observed shoulder can be ascribed to the presence of the cubic Mg_2NiH_4 following Rietveld amounts in Fig.1 and ESI Fig.S2.

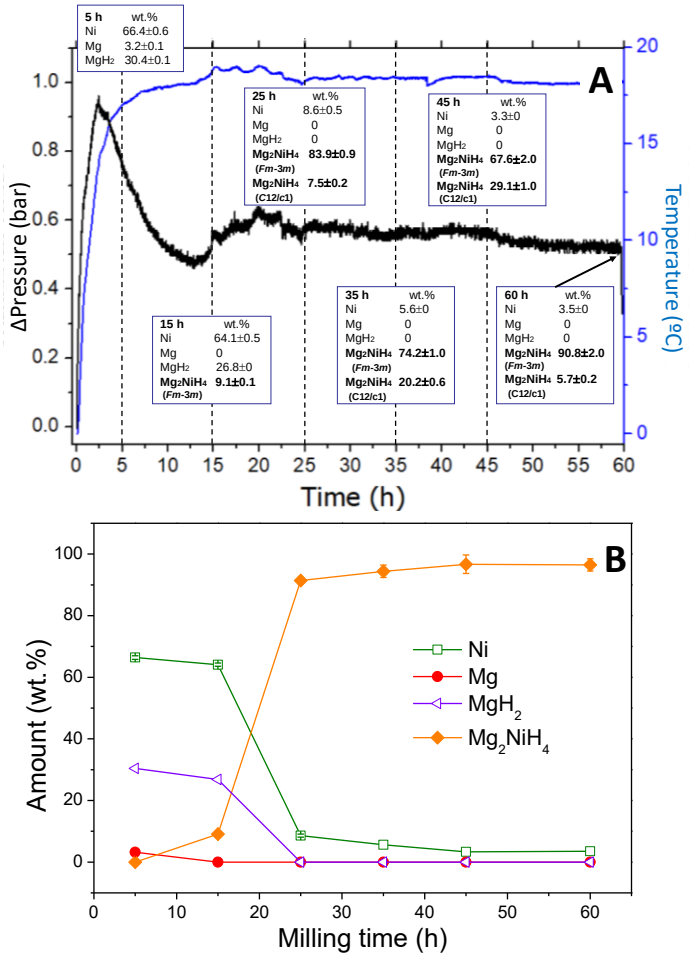

Fig. 1*In situ* monitoring mechanical milling and Rietveld analyses results: **A** Temperature and pressure evolution during the milling process of the 2MgH_2-Ni stoichiometric powder mixture and quantitative phase results based on Rietveld analyses, **B** Phase amounts trends based on Rietveld analyses (Mg_2NiH_4 as the total amount of the two polymorph species).

The HP-DSC curve obtained for the material milled 25 hours (Fig. S4) shows two endothermic events. The small and broad event starting before the phase transition temperature (~230 ºC) at about 200 ºC can be associated with the early decomposition of LT1-Mg_2NiH_4, as reported by Rönnebro *et al.*[38]. The phase transition from LT- to HT-Mg_2NiH_4 is not observed in the DSC-curve (ESI Fig.S4) due to the overlapping with the decomposition of LT1. The second thermal event is considerably more significant than the first one (Fig. S4) and presents a peak maximum at about 290 ºC. This single thermal event can be ascribed to the dehydrogenation of the cubic Mg_2NiH_4 (HT). For this sample, PXD and Rietveld results (Fig. 1, Fig. S2) are in good accordance with the proposed interpretation of the thermal behavior after 25 hours of milling since reflections from the LT1 phase are detected and the material is composed of a small amount of LT1 phase.

Finally, the HP-DSC curve obtained for the material milled 60 hours (ESI Fig. S4) shows the broad endothermic event between 180 ºC and 250 ºC ascribed to the LT1-Mg_2NiH_4 decomposition, and two overlapped endothermic events between 275 ºC and 325 ºC. It is possible to observe a small event with a peak maximum at ~280 ºC. As reported in the literature[38], this small endothermic event can be attributed to the second H_2 release from LT1-Mg_2NiH_4. The second and more significant endothermal event with a peak maximum at ~295 ºC accounts for the cubic Mg_2NiH_4(HT) dehydrogenation. It is essential to mention that the observed overlapped thermal events are not seen in the sample milled for 25 hours despite higher amount of LT1-Mg_2NiH_4. This fact might be due to the microstructural properties of the material, and it will be further discussed.

Fig. 2 shows SEM micrographs, Ni and Mg mapping after 5 h and 60 h, plus a table that reports the mean particle size of the material after each milling period. All the histograms, SEM photos and mapping pictures are exhibited in ESI: Fig.S5. It is possible to observe that the particle size of the material decreases from 20 µm to about 10 µm during the first 30 hours of milling and then starts to increase until reaching about 47 µm for the as-milled material. The mapping pictures confirm an intimate mixture between the phases containing Ni and Mg.

From the diffractograms obtained for the material upon milling, the crystallite sizes were calculated, and the trend shown in the ESI: Fig. S6. The crystallite size of MgH_2 is reduced from about 75 nm to about 15 nm until it is consumed during the first 15 hours. Additionally, Ni reduces its crystallite size from about 65 nm down to less than 5 nm after 45 hours of milling. Once the most abundant polymorph of Mg_2NiH_4 (cubic) is formed, its crystallite size remains unchanged (~10 nm).

3.2 CO_2 capture and conversion by as-milled Mg_2NiH_4 interaction

Investigations on the CO_2 capture and conversion *via* Mg_2NiH_4 decomposition were performed by heating in static conditions. Gaseous products were characterized by FTIR spectroscopy, while solid products were analyzed by Raman spectroscopy and PXD technique. Fig. 3 shows a comparison between the normalized FTIR spectra measured for the gaseous products of the as-milled Mg_2NiH_4-CO_2 system and for the as-sintered Mg_2NiH_4-CO_2 system studied in our previous work[16]. After the thermal treatment under CO_2 atmosphere (4:1 H_2:CO_2 mol ratio) at 400 ºC for 5 hours, it is possible to observe that in both cases, the main product is CH_4. The relative intensity of the spectra denotes that the as-milled Mg_2NiH_4-CO_2 system appears to produce a smaller amount of CH_4 than the as-sintered Mg_2NiH_4-CO_2 system. However, the FTIR spectrum of the as-milled Mg_2NiH_4-CO_2 system does not show the presence of CO_2 and CO (Fig. 3(a)), while the as-sintered Mg_2NiH_4-CO_2 system does (Fig. 3(b)).

Fig. 4 presents PXD analyses of Mg_2NiH_4 after different thermal processes: in Ar flow and heating in static conditions under CO_2 atmosphere (4:1 H_2:CO_2 mol ratio). After dehydrogenation under Ar flow (Fig. 4(a)), the crystalline phases present in the investigated specimen are mainly Mg_2Ni and Ni. Nevertheless, the crystalline phases after the CO_2 interaction under static conditions are Mg_2Ni, Ni, MgO, and $MgNi_2$.

Fig. 5 shows Raman spectra of the as-milled Mg_2NiH_4-CO_2 and as-sintered Mg_2NiH_4-CO_2 system after the thermal process in static conditions. It is possible to observe the presence of just two peaks belonging to in-plane vibrations of the sp^2 domain of graphite (G mode at 1590 cm^{-1}) and defects and disorders of carbonaceous solid (D mode at 1341 cm^{-1})[39].Comparing the Raman results, it is clear that no graphite species is present in the as-sintered Mg_2NiH_4-CO_2 system. However, FT-IR detected carbonate species after the methanation process[16].

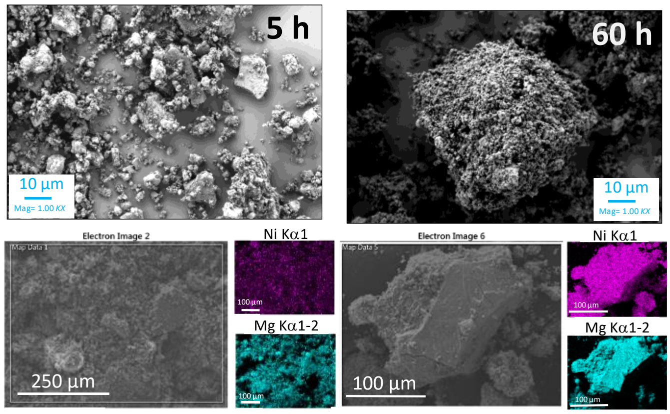

Milling time (h)	Particle mean size (µm)
5	20
10	20
20	15
30	10
35	17
40	17
50	20
60	47

Fig. 2 SEM observations and Mg and Ni mapping upon milling, and Particle size distribution (PSD) for the $2MgH_2$-Ni stoichiometric powder mixture.

4. Discussion

4.1 Mg_2NiH_4 synthesis and decomposition under non-reactive atmosphere

The synthesis of Mg_2NiH_4 was carried out by *in situ* monitoring mechanical milling. Fig. 1 shows the temperature and gaseous pressure curves recorded during the milling. To better understand the phenomena occurring during milling, a milling process without material was carried out in the same conditions (initial H_2 pressure, temperature, kind and amount of grinding medium). This experiment is hereafter called the "white process". As shown in ESI Fig.S7, for the white process, both temperature (T) and pressure (P) increase during

the first two hours and then remain stable. The rise of pressure in the empty milling chamber accounts for the rise of temperature in the vial during milling. Once a stable temperature is reached, the pressure remains constant. It is noteworthy that mechanical work is still provided after achieving constant temperature and pressure conditions. Therefore, taking into account that the milling chamber is made of stainless steel, which has a relatively high thermal conductivity, it is possible to assume that this behavior is related to the thermal equilibrium reached between the milling system and the environment: all the mechanical work converted in heat is dissipated through the milling chamber surface.

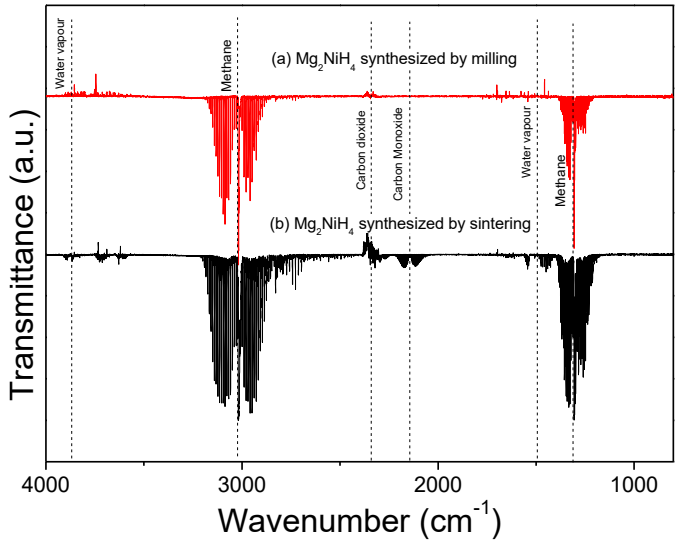

Fig. 3 FTIR spectra of the gas products for the interaction for (a) as-milled Mg_2NiH_4 after CO_2 interaction at 400 °C for 5 h and (b) Mg_2NiH_4 synthesized by sintering after CO_2 interaction at 400 °C for 5 h[16]. For both samples H_2:CO_2= 4:1 mol ratio. CH_4 bands: C-H bending in the range from 1204 to 1390 cm^{-1} and C-H stretching in the range from 2818 to 3181 cm^{-1}.

The rise of temperature (ΔT~ 24 °C, ESI Fig.S7(b)) and pressure (ΔP~ 2.2 bar, ESI Fig.S7(a)) during the first 2 hours in the white process is larger than that observed during the synthesis process (ΔT~ 19 °C, ESI Fig.S7(d); ΔP~ 1.0 °C, ESI Fig.S7(c)). This suggests that part of the mechanical energy transferred by the grinding medium to the material during milling is partially used for supporting the synthesis of Mg_2NiH_4 and for refining the material microstructure. During the synthesis process, after the initial period of 2 hours (Fig.1A, ESI Fig.S7(c)), the pressure drops about 0.5 bar. As seen in the PXD patterns (ESI Fig.S2) and the phase quantification obtained for the material milled 5 hours (Fig.1, ESI Table S1), an amount of 3.2±0.1 wt.% of free Mg is detected. Considering the decrease of 0.5 bar of H_2 pressure in the milling period between ~2 hours to ~13 hours and assuming that all the consumed hydrogen is used to form MgH_2 from the observed free Mg, an overall amount of ~2.9 wt.% of free Mg is calculated by applying the ideal gas equation (ESI – Calculations of Mg hydrogenation), which is quite in accordance with the one obtained from the Rietveld analyses (Fig.1, ESI Table S1).

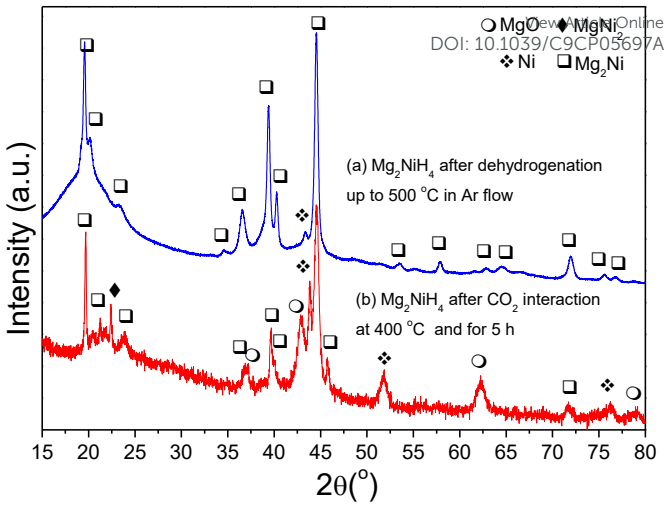

Fig. 4 PXD patterns for (a) as-milled Mg_2NiH_4 after dehydrogenation in Ar flow at a heating rate of 3 °C/min and up to 500 °C and (b) as-milled Mg_2NiH_4 after CO_2 interaction at 400 °C for 5 h.

After 15 hours of milling, the characterization of the solid product does not show the presence of free Mg (ESI Fig.S2, Fig.1, ESI Table S1). Thus, the hydrogenation of free Mg coming from the starting material explains the initial drop of H_2 pressure during the initial phases of the synthesis process (Fig.1, ESI Fig.S7). After 15 h of milling time, the cubic Mg_2NiH_4 (S.G. *Fm*-3*m*) is already present. It was reported that the cubic Mg_2NiH_4, known as the HT phase, can be produced by mechanical milling since the structural transition from LT to HT is strongly disturbed by internal stress induced by mechanical work[24,40].It was proposed that the cubic phase produced at room temperature by mechanical stress or pressure is a pseudo-HT cubic structure with a cell parameter of 6.54 Å[25]. However, it was also found that the HT-Mg_2NiH_4 cubic phase with a cell parameter of 6.507 Å[41]can be synthesized by ball milling[40]. Rietveld analyses here show a proper fitting with the cubic HT-Mg_2NiH_4 with cell parameter of 6.507 Å (CIF file 162412; Fig. 1, Fig.S1 and Table S1), in agreement with the abovementioned works[40,41]. Further milling leads to the synthesis of small amounts of LT1–Mg_2NiH_4 phase, i.e. without microtwinning. It is noted that the LT1-Mg_2NiH_4 starts to be formed after 20 hours of milling and increases in quantity up to 45 hours from 7.5±0.2 wt.% to 29.1±1.0 wt.% (Fig.1 and Fig.S2). The decompression of the cubic phase leads to the transformation back to LT-phase[42]. Therefore, this suggests that the formed HT–Mg_2NiH_4 particles reduce the structural stress by braking and reducing the particle size from 20 µm to 10 µm between 10 hours and 30 hours of mechanical milling (Fig. 2). Then, between 30 hours and 45 hours of milling the particle size increases, but remains below 20 µm. Hence, in our case the formation and increase of LT1–Mg_2NiH_4 can be related to the stress release owing to the particle size reduction as well as to the inefficient energy transfer from the grinding media to the powder, causing the relaxation of the material. After 40 – 45 hours of milling, the particle size markedly increases over 45 µm, and the material becomes coarse. Finally, after 60 hours of milling the amount of LT1–Mg_2NiH_4 notably decreases down to 5.7±0.2 wt.%. This fact can be related to an increase of compression due to the agglomeration of the particles, which results in the transformation of the LT1–Mg_2NiH_4 back to the HT–Mg_2NiH_4. An analysis of the crystallite size was also done (ESI Fig.S6), but there is no trend upon the whole process since it remains in about 10 nm for the HT–Mg_2NiH_4. Another significant feature is the presence of the LT1–Mg_2NiH_4 (without microtwinning) instead of the LT2–Mg_2NiH_4 (with

microtwinning). It was found that the presence of free Mg suppresses the creation of microtwinning, while the presence of MgH_2 reduces its amount[43]. Thus, the formation of the LT1–Mg_2NiH_4 might be promoted by the initial presence of free Mg and MgH_2 up to about 13 hours and 25 hours of milling, respectively (Fig.1, Fig.S2). DSC curves (ESI Fig.S4) after 25 hours and 60 hours of milling are in concordance with the Mg_2NiH_4 polymorphs observed in the PXD analyses. The higher decomposition temperature and double endothermic event in the DSC curve at 60 hours of milling can be related to the coarse condition of the material since this condition generates more considerable diffusion constraints for hydrogen release.

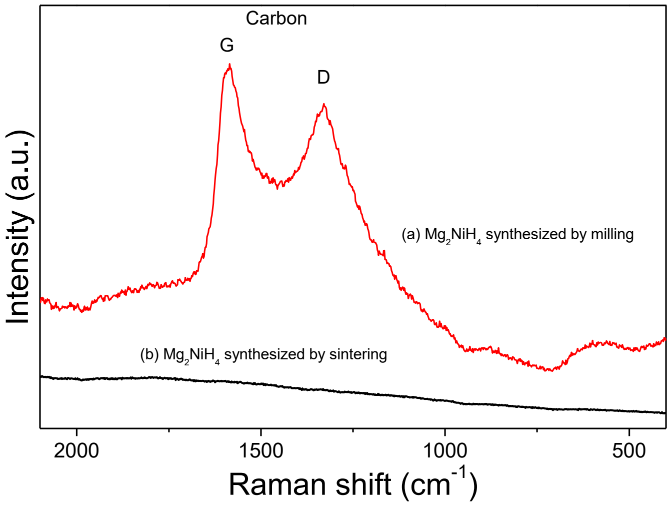

Fig. 5 Raman spectroscopy for the solid phase for (a) as-milled Mg_2NiH_4 after CO_2 interaction at 400 ºC for 5 h and (b) Mg_2NiH_4 synthesized by sintering after CO_2 interaction at 400 ºC for 5 h[16].

The material after milling contains a total amount of about 96 wt.% of Mg_2NiH_4, taking into account both polymorphs, and remnant Ni. According to our results and analyses, and in agreement with previous works[24,40], the synthesis reaction proceeds according to reaction (2):

$$2MgH_{2(s)} + Ni_{(s)} \rightarrow Mg_2NiH_{4(s)} \quad (2)$$

The decomposition of the formed complex hydride under H_2 atmosphere can be described based on the volumetric measurements (ESI Fig.S3), DSC curves (ESI Fig.S4) and PXD results (Fig.4(a)). It is possible to describe the primary dehydrogenation process in a non-reactive atmosphere as described in reaction (3), providing H_2 and Mg_2Ni as main phases, in agreement with the literature[37].

$$Mg_2NiH_{4(s)} \rightarrow Mg_2Ni_{(s)} + 2H_{2(g)} \quad (3)$$

4.2 Methanation of CO_2 *via* HT–Mg_2NiH_4 decomposition

In our recent work[16], the optimal conditions for the methanation reaction of CO_2 *via* complex hydride decomposition were determined based on experimental results and thermodynamic calculations. It was found that 400 ºC and $4H_2$:$1CO_2$ stoichiometric ratio conditions are required for the CO_2 methanation through complex hydride decomposition. In the case of as-sintered Mg_2NiH_4 with monoclinic structure, full conversion was reached after 10 hours with the formation of CO as an intermediate gas product, and with the partial decomposition of the complex hydride[16]. Herein, full methanation of CO_2 is achieved in 5 hours *via* the complete decomposition of as-milled Mg_2NiH_4 with cubic structure at the same defined optimal conditions, and the formation of CO is not evidenced (Fig.3). On the one hand, CO might have formed and decomposed during the methanation process. On the other hand, graphite is present in the solid phase at the end of the process. These results suggest that the global mechanism for the methanation *via* as-milled Mg_2NiH_4 is faster and different from the one *via* as-sintered Mg_2NiH_4.

Mass spectroscopy measurements for the interaction of the as-sintered Mg_2NiH_4 and CO_2 showed a reaction zone in the temperature between 350 ºC and 410 ºC[16]. Under non-reactive atmosphere and dynamic conditions, the as-sintered Mg_2NiH_4 presents higher decomposition temperatures (325 ºC – 400 ºC) than the as-milled Mg_2NiH_4(200 ºC - 325 ºC), ESI: Fig.S8. It was already reported that the hydrogen release significantly increases at about 180 ºC[44]. After the phase transition from LT to HT Mg_2NiH_4 at about 230 ºC, the metallic state of Mg increases on the complex hydride surface[15]. In our case, the as-milled Mg_2NiH_4 has a cubic (HT) structure even at room temperature; hence, its surface is more reactive from the beginning of the decomposition process. Taking into account the lower range of decomposition temperature and higher surface reactivity, it is highly possible that the as-milled Mg_2NiH_4 already decomposes under $CO_{2(g)}$ atmosphere at the time to reach 400 ºC. Calculations on the equilibrium compositions were done considering the experimental conditions: $4H_2$:$1CO_2$ stoichiometric ratio, 400 ºC, constant pressure of 1.2 bar in a constant volume of about 10 cm^3, and variable hydrogen pressure up to 1.2 bar in the same volume. Both calculations approach provided similar results (ESI Fig. S9). Fig. 6 exhibits the evolution of the equilibrium amounts as a function of the pressure at 400 ºC. All curves are shown from the beginning of the methanation process, having available 4 mol of $H_{2(g)}$and under the set conditions $CO_{2(g)}$ already decomposed. Additionally, the table on the right side of Fig. 6 shows the final equilibrium composition from the final state of the calculation at 400 ºC and 1.2 bar of pressure. As seen, the calculations indicate that $CO_{(g)}$ is not formed and not remnant $CO_{2(g)}$ is left. $C_{(s)}$ comes from $CO_{2(g)}$ decomposition, and finally, a small amount of $C_{(s)}$ remains in agreement with the results shown in Fig. 3 and 5.

The calculations do not predict the formation of gaseous water (steam) and carbonate species. In this regard, quite weak signals of steam are seen by FTIR (Fig.3) and no carbonate species are detected by PXD or evidenced by Raman spectroscopy. Previous works reported the formation of carbonate surface oxide layers on Mg to promote the methanation[45,46]. However, the G and D modes of graphite are detected, as shown in Fig. 3[39], and as well as for the Mg_2FeH_6-CO_2 system[16]. This suggests that the cubic polymorph form of $Mg_2NiH_{4(s)}$ promotes the CO_2 chemisorption on basic MgO layers. The calculations also predict the formation of a small amount of $MgH_{2(s)}$, but it is not verified experimentally, since either its amount is below the detection limit or it is not present (Fig. 4).

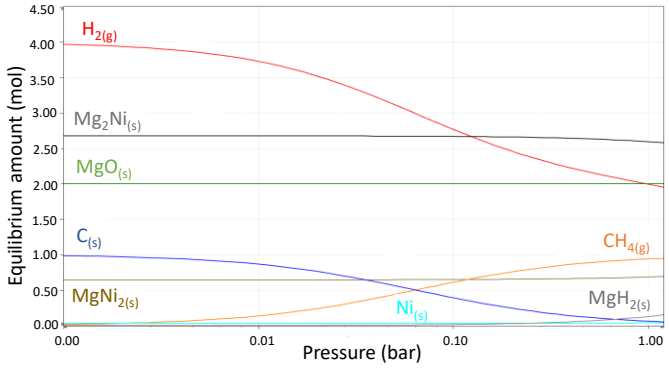

Equilibrium Amount at the end of the process (400 ºC and 1.2 bar)

Species	Mol	Mol%	Species	Mol	Mol%
$CO_{2(g)}$	0.0	0.0	$Ni_{(s)}$	0.04	0.60
$H_{2(g)}$	2.05	32.0	$CH_3OH_{(g)}$	0.00	0.00
$Mg_2Ni_{(s)}$	0.65	10.0	$C_{(s)}$	0.05	0.70
$MgNi_{2(s)}$	0.65	10.0	$MgO_{(s)}$	2.00	31.0
$O_{2(g)}$	0.00	0.00	$MgCO_{3(s)}$	0.00	0.00
$CO_{(g)}$	0.00	0.00	$NiCO_{3(s)}$	0.00	0.00
$H_2O_{(g)}$	0.00	0.00	$H_2O_{(l)}$	0.00	0.00
$CH_{4(g)}$	0.95	15.0	$C_2H_{6(g)}$	0.00	0.00
$C_2H_{4(g)}$	0.00	0.00	$MgH_{2(s)}$	0.05	0.70

Fig. 6 Equilibrium amounts of phases calculated at 400 °C, $4H_2$:$1CO_2$ stoichiometric ratio and variable pressure up to 1.2 bar.

Several theoretical and experimental investigations on the methanation mechanism of CO_2 have been performed[47-49]. The discussion still falls into the same controversy: methanation of CO_2 through the formation of CO as intermediate or direct methanation without CO formation. There are three typical pathways for the methanation process: 1) direct dissociation of into an activated intermediate adsorbed CO*, 2) formate (HCO_2^-) pathway *via* C-terminal hydrogenation to the adsorbed species HCOO* and 3) carboxyl pathway *via* O-terminal hydrogenation to the adsorbed species COOH*[47,48,50]. In the case of Ni as the catalyst, Ni(111) facet is the most active surface for the CO_2 methanation[51]. DFT calculations on the reaction mechanism for the CO_2 methanation on Ni-based catalyst showed different pathways[48,52-54]. On the one hand, the methanation through the formation of CO* on Ni(111) was proposed[48]. On the other hand, it was also suggested that CO_2 dissociates into an activated carbon species C* on Ni(111) surface, and then C* hydrogenates to CH_4[52]. Recently, it was shown that the presence of MgO changes the methanation pathway on Ni(111) catalyst[53]. The optimal pathway changes from the formate pathway (HCOO*) on pure Ni(111) to the formation of H_2COO* as intermediate species on Ni supported on MgO. Moreover, MgO promotes the methanation reaction and eases the formation of H_2O upon methanation owing to the H-spillover effect and the strong adsorption of OH[53]. In our case, it seems to be that the mechanism is slightly different from the proposed for the Ni/MgO system, since the formation of steam is minimal and it is not predicted (Fig. 6). It is not possible to have a deep insight into the elemental reaction pathways. However, a different mechanism accounts for a different catalyst-support interaction, which affects the methanation pathway, activity, and selectivity[54,55].

Based on the experimental results and calculations, a global mechanism for the as-milled Mg_2NiH_4-CO_2 interaction and methanation can be proposed. Under static conditions and at the beginning of the process, both $Mg_2NiH_{4(s)}$ and $CO_{2(g)}$ can decompose according to reaction (4). This reaction is thermodynamically favored under the experimental conditions (ESI Table S2), and it is in good agreement with the stoichiometry, and phases found experimentally as well as the obtained calculation outcomes. Even though this process might have started before reaching 400 °C, during the temperature ramp, the high reactivity of $Mg_2NiH_{4(s)}$towards $CO_{2(g)}$was observed at 400 °C or higher[15,16]. Therefore, $CO_{2(g)}$ can be first adsorbed on the cubic complex hydride surface with a high degree of Mg in the metallic state and a small amount of Ni particles available (Fig. 1 – composition after milling) for the CO_2 activation and cleavage[4-7,15]. Then, the disproportionation of the hydride complex surface leads to the formation of Ni-$MgNi_2$-Mg_2Ni/MgO catalyst, on which $CO_{2(g)}$ is strongly adsorbed because of the fundamental properties of MgO as catalyst support[9]. The proposed global mechanism suggests that the methanation pathway can occur by the intermediate formation of adsorbed C* and the direct formation of CH_4 as proposed by Ren et al.[52]. Therefore, finally, two moles of $H_{2(g)}$ can react with one mol of $C_{(s)}$ through conventional gasification of a solid, according to reaction (5). At the end of the methanation process and considering the $4H_2$:$1CO_2$ stoichiometry, the excess of hydrogen predicted in the calculations agrees with reaction (5). This methanation global mechanism is proposed as the main one. Nonetheless, secondary reactions such as the Sabatier and water gas shift reaction (WGS), involving H_2O and CO, might also occur in a quite small degree. Although the cubic $Mg_2NiH_{4(s)}$ fully decomposes, the consumption of neither $H_{2(g)}$ nor $C_{(s)}$ is complete. In the case of $C_{(s)}$, this is verified by the Raman spectrum (Fig. 5(a)). The slightly lower intensity of $CH_{4(g)}$ in the gas FTIR spectrum of as-milled $2Mg_2NiH_{4(s)}$-$CO_{2(g)}$ system (Fig. 3(a)) in comparison spectrum of the sintered $2Mg_2NiH_{4(s)}$-$CO_{2(g)}$ system with the (Fig. 3(b)) can be attributed to Ni and Ni-based alloys deactivation caused by coke deposition (Fig. 5(a))[7-11].

$$2Mg_2NiH_{4(s)} + CO_{2(g)} \rightarrow 0.75Mg_2Ni_{(s)} + 2MgO_{(s)} + 0.25Ni_{(s)} + 0.5MgNi_{2(s)} + C_{(s)} + 4H_{2(g)} \quad (4)$$

$$C_{(s)} + 2H_{2(g)} \leftrightarrows CH_{4(g)} \quad (5)$$

5. Conclusions

The synthesis of Mg_2NiH_4 by *in situ* monitoring mechanical milling and the reactivity of this as-milled nickel complex hydrides toward CO_2 methanation has been investigated. *In situ* monitoring milling technique allows understanding the synthesis process. Internal stress induced by mechanical work leads to the synthesis of the Mg_2NiH_4 with cubic structure (S.G. *Fm*-3*m*) from the beginning of the process. During the milling process, different amounts of the monoclinic polymorph of Mg_2NiH_4 (S.G. *C*12/*c*1) are also observed due to compression

and relaxation of the cubic phase. At the end of the milling process, the material is composed of 90.8 wt.% of cubic Mg_2NiH_4, 5.7 wt.% of monoclinic Mg_2NiH_4, and 3.5 wt.% of remnant Ni. Assessment of the reactivity of as-milled Mg_2NiH_4 towards CO_2 methanation shows a different behavior in comparison with Mg_2NiH_4 obtained by sintering[16]. Under static conditions at 400 °C, the as-milled Mg_2NiH_4-CO_2 system provides CH_4 from the full CO_2 consumption in 5 hours. Studies on the global mechanism suggest that the higher reactivity of nanostructured cubic Mg_2NiH_4 results in its fast decomposition under CO_2 atmosphere, providing a Ni-Mg_2Ni-$MgNi_2$/MgO catalytic system for the methanation reaction. Experimental results and thermodynamic calculations suggest that the leading global methanation mechanism undergoes by the adsorption of C and the direct solid gasification towards CH_4 formation. Remnant C can cause passivation of the conversion active phases, resulting in lower amounts of produced methane. To the best of our knowledge, this is the first investigation reported in literature on the influence of the synthesis on the catalyst-support interaction *via* Ni metal complex hydride on the methanation global mechanism and opens new horizons in the development of new materials for CO_2 capture and conversion purposed.

Conflicts of interest

There are no conflicts to declare.

Acknowledgments

The present work is part of the CO2MPRISE, "CO_2 absorbing Materials Project- RISE", a project that has received funding from the European Union's Horizon 2020 research and innovation programme, under the Marie Skłodowska-Curie Grant Agreement No 734873. The work was also supported by CONICET (Consejo Nacional de Investigaciones Científicas y Técnicas), ANPCyT– (Agencia Nacional de Promoción Científica y Tecnológica), CNEA (Comisión Nacional de Energía Atómica) and HZG (Helmholtz–ZentrumGeesthacht). The authors also thank Bernardo Pentke (Departamento Fisicoquímica de Materiales) for the SEM micrographs and Sebastián Anguiano for the Raman measurements (Laboratorio de Fotónica y fotoelectrónica).

References

1 W. Wang and J. Gong, *Front. Chem. Sci. Eng.*, 2011, **5**, 2‑10.
2 V. C. Miguel, A. Mendes, L. M. Madeira, *Energies*, 2018, **11**, 3259(20).
3 P. Sabatier, J.B. Senderens, *Acad. Sci. Paris,*1902, **134**, 514-516.
4 T. Schaaf, J. Grünig, M. Roman Schuster, T. Rothenfluh, A. Orth, *Energy Sustain Soc*.,2014, **4 (1)**, 2–14.
5 J. Gao, Q. Liu, F. Gu, B. Liu, Z. Zhong, F. Su, *RSC Adv.*, 2015, **5**, 22759–22776.
6 H. Wang, Y. Pei, M. Qiao, B.Zong, *Catalysis*, 2017, **29**, 1–28.
7 Lui, C.; Cundari, T.R.; Wilson, A.K. CO_2 reduction on Transition Metal (Fe, Co, Ni and Cu) surfaces: In comparison with Heterogeneous Catalysis. *J Phys. Chem. C*, 2012, **116**, 5681-5688.
8 S. Tada, T. Shimizu, H. Kameyama, T. Haneda, R. Kikuchi, *Int. J. Hydrogen Energy*, 2012, **37**, 5527-5531.
9 M.Guo, G.Lu, *Catal. Commun*. 2014, **54**, 55–60.
10 M. Younas, L.L. Kong, M.J.K. Bashir, H. Nadeem, A. Shehzad, S. Sethupathi, *Energy Fuels,*2016, **30**, 8815-8831.
11 S. De, J. Zhang, R. Luque, N. Yan, *Energy Environ. Sci*.,2016, **9**, 3314-3347
12 P. Selvam, B. Viswanathan, V. Srinivasan, *J Less Common Met.*, 1990,**158**, L1-L7.
13 P. Selvam, B. Viswanathan, V. Srinivasan, V. *Int J Hydrogen Energy*,1990, **15 (2)**, 133-137.
14 G. Mulas, R. Campesi, S. Garroni, F. Delogu, C. Milanese, *Appl. Surf. Sci.*, 2011, 257, 8165–8170.
15 K. Kato, K.; A. Borgschulte, D. Ferri, M. Bielmann, J-C. Crivello, D. Wiedenmann, M. Parlinska-Wojtan, P. Rossbach, Y. Lu, A. Remhofa, A. Zuttel, *Phys. Chem. Chem. Phys.*, 2012, **14**, 5518–5526.
16 M. L. Grasso, J. Puszkiel, L. Fernández Albanesi, M. Dornheim, C. Pistidda, F. C. Gennari, *Phys. Chem. Chem. Phys.*, 2019, **21**, 19825-19834.
17 J. J. Didisheim, P. Zolliker, K. Yvon, P. Fischer, J. Schefer, M. Gubelmann, A. F. Williams, Inorg. Chem., 1984, **23**, 1953-1957.
18 T. Massalski,H. Okamoto, P.R. Subramanian, L. Kacprzak (Eds.), Binary Alloy Phase Diagrams, second ed., American Society for Metals, Metals Park, OH, 1990.
19 P. Zolliker, K. Yvon, C.H. Baerlocher, J. Less-Common Met., 1986, **115**, 65-78.
20 J.J. Reilly, R.H. Wiswall Jr., *Inorg. Chem.*, 1968, **7**, 2254-2256.
21 J. Schefer, P. Fischer, W. Hälg, F. Stucki, L. Schlapbach, J.J Didisheim, K. Yvon, A.F. Andresen, *J. Less-Common Met.*, 1980, **74**, 65-73.
22 P. Zolliker, K. Yvon, J. D. Jorgensen, F. J. Rotella, *Inorg. Chem.,* 1986,**25 (20)**, 3590-359.
23 Z. Gavra, M. H. Mintz, G. Kimmel, Z. Hadari, *Inorg. Chem.,*1979, **18 (12)**, 3595-3597.
24 E. Rönnebro, J.O. Jensen, D. Noréus, N.J. Bjerrum, *J. Alloys Comp.*, 1999, **293**, 146-149.
25 S. Yamamoto, Y. Fukai, E. Rönnebro, J. Chen, T. Sakai, *J. Alloys Comp.*, 2003, **356-357**, 697-700.
26 D. Noréus, L. Kihlborg, *J. Less Common Metals*, 1986, **123**, 233-239.
27 H. Blomqvist, D. Noréus*, J. Appl. Phys.*, 2002, **91**, 5141-5148.
28 H. Blomqvist, D. Noréus*,* O. Babushkin, F. Nion, E. Vourien, J. Mater Sci. Lett,. 2003, **22**, 1487-1505.
29 Bergerhoff G, Brown I D. Crystallographic databases (ICSD). Int Union Crystallogr 1987.
30 H. M. Rietveld, J. Appl. Crystallogr., 1968, **2**, 65–71.
31 L. Lutterotti, *Nucl. Instruments Methods Phys. Res. Sect. B Beam Interact. with Mater. Atoms*, 2010, **268 (3–4)**, 334–340.
32 L. Alexander, P.H. Klug, *J. Appl. Phys.*, 2004, **21**, 137.
33 R. Schulz, J. Huot, S. Boily, Can. Patent (1999) Ser. e Nr. 2207149.
34 HSC Chemistry9.7, For Windows, Outotec.
35 N. Hanada, T. Ichikawa, H. Fujii, *J. Phys. Chem. B*, 2005, **109**, 7188-7194.
36 J.A. Puszkiel, F.C. Gennari, *ScriptaMaterialia*, 2009, **60**, 667‑670.
37 J.J. Reilly, R.H. Wiswall, *Inorg. Chem.*, 1968, **7**, 2254-2256.
38 E. Rönnebro, D. Noréus*,* Appl. Surf. Sci., 2004, **228**, 115–119.
39 J. Hong, M.K. Park, E.J., D. E.Lee, D. S. Hwang, S. Ryu, *Scientific Reports,* 2013, **3**, 2700.
40 R.Martinez-Coronado, M. Retuerto, J.A. Alonso, *Int. J. Hydrogen Energy*, 2012, **37**, 4188-4193.

View Article Online
DOI: 10.1039/C9CP05697A

41 J. Zhang, D.W. Zhou, L.P. He, P. Peng, J.S. Lui, *J. Phys. Chem. Solids*, 2009, **70**, 32-39.
42 E. Rönnebro, Y. Fukai, S. Yamamoto, T. Sakai, *J. AlloysCompd.*, 2004, **385**, 276-282.
43 H. Blomqvist, E. Rönnebro, D. Noréus, T. Kuji, *J. Alloys Compd.*, 2002, **330-332**, 268-270.
44 S. Ono, Y. Ishido, K. Imanari, T. Tabata, Y. K. Cho, R. Yamamoto and M. Doyama, *J. Less-CommonMet.*, 1982, **88**, 57.
45 E. Akiba and S. Ono, *J. Less-Common Met.*, 1986, **124**, L1-L4.
46 J. N. Park and E. W. A. McFarland, *J. Catal.*, 2009, **266**, 92–97.
47 M.A.A. Aziz, A.A. Jalil, S. Triwahyono, A. Ahmad, *Green Chem.* 2015, **17**, 2647–2663
48 H. Yuan, X. Zhu, J. Han, H. Wang, Q. Ge, *J. CO_2 Util.*, 2018,**26**, 8–18
49 P. Frontera, A. Macario, M. Ferraro, P. Antonucci, Catalysts, 2017, **7**, 59 (28).
50 S. Kattel, P. Liu, J.G. Chen, *J. Am. Chem. Soc.*, 2017, **139**, 9739–9754.
51 W.L. Zhen, F. Gao, B. Tian, P. Ding, Y.B. Deng, Z. Li, H.B. Gao, G.X. Lu, *J. Catal.*, 2017, **348**, 200–211.
52 J. Ren, H.L. Guo, J.Z. Yang, Z.F. Qin, J.Y. Lin, Z. Li, *Appl. Surf. Sci.*, 2015, **351**, 504–516.
53 Jin Huanga, Xiao Lia, XiangWanga, Xiuzhong Fanga, HongmingWangb, XianglanXua, *J. CO_2 Util.*, 2019, **33**, 55–63.
54 P.A.U. Aldana, F. Ocampo, K. Kobl, B. Louis, F. Thibault-Starzyk, M. Daturi, P. Bazin, S. Thomas, A.C. Roger, *Catal. Today*, 2013, **215**, 201–207.
55 M. Li, H. Amari, A.C. van Veen, *Appl. Catal. B*, 2018, **239**, 27–35.